

Impact of Ge, Ga, and Al doping on the mechanical properties and anisotropy of Cr₃Si: a first-principles investigation

Siavash Karbasizadeh¹ and Mohammad Amirabbasi²

¹*Materials Department, University of California, Santa Barbara, California 93106-5050, USA*

²*Technical University of Darmstadt, Materials Modelling Division,
Otto-Berndt-Straße 3, Darmstadt D-64287, Germany*

(Dated: August 14, 2024)

The mechanical properties of cubic Cr₃Si doped with Ge, Ga, and Al are systematically investigated using first-principles calculations based on density functional theory. We examine the effects of doping on the lattice constants, formation enthalpies, elastic moduli, wave velocities, Debye temperature, and mechanical anisotropy to understand how these dopants influence the structural stability and mechanical behavior of Cr₃Si. Our results indicate that doping with Ge, Ga, and Al lead to an increase in lattice constants, reflecting lattice expansion. Despite the negative formation enthalpies across all doped configurations, indicating thermodynamic stability, higher dopant concentrations reduce the stability of the alloys. The elastic moduli, including bulk modulus, shear modulus, and Young's modulus, decrease with increasing dopant concentration, suggesting a reduction in mechanical stiffness and rigidity. Wave velocity and Debye temperature also grow smaller, further indicating a softer material structure with diminished thermal conductivity. Additionally, the study reveals that Al and Ga doping significantly increases mechanical anisotropy, as demonstrated by the anisotropy indices and three-dimensional contour analyses. In contrast, Ge maintains a more isotropic mechanical behavior, making it the most favorable dopant for applications requiring balanced mechanical and thermal properties. These findings provide critical insights into the design and optimization of Cr₃Si-based materials, highlighting the trade-offs between mechanical strength, anisotropy, and other functional properties introduced by doping. The results underscore the potential of tailoring Cr₃Si alloys for specific high-performance applications where directional mechanical properties and thermal stability are of paramount importance.

I. INTRODUCTION

The Cr-Si binary silicides have received great attention due to their high thermal stability and excellent mechanical properties [1]. Owing to their better oxidation resistance over their silicide counterparts, their usage in the industry has been extensive [2]. Of the binary phases of Cr-Si, the cubic Cr₃Si phase stands out [3–10]. It has been reported to be stable in a temperature range down to 6 K [4, 5] with a Pauli paramagnetic behavior in the temperature range between 4.2 and 300 K [6]. Cr₃Si provides a high melting point ($T_m > 1700$ °C), high temperature strength, and high creep resistance [7, 8]. Recent investigations have also shown this structure to have a promising oxidation and nitridation resistance at ultra-high temperatures ($T > 1200$ °C) [9, 10]. This intermetallic system, however, does not meet all the criteria for high-temperature structural applications. Of the requirements lacking in this material are high microstructural thermal stability, and room-temperature ductility and toughness [11, 12].

According to geometric point, this cubic structure belongs to an A15 cubic structure with a space group of $Pm\bar{3}n$ in which Cr and Si occupy 6c (0.25, 0, 0.5) and 2a (0, 0, 0) of the Wyckoff positions, respectively (Fig. 1). One of the prime approaches to modify and tune the efficiency of this system is alloying which has seen some interesting improvement of characteristics in the structure to alleviate the deficiencies. Soleimani-Dorcheh *et al.* [9] showed through measurements that incorporating

Ge into the material in small concentrations, substituting Si, can reduce the oxidation and evaporation rates. Raj [8, 13] concluded that an alloy of Mo and Cr₃Si can be utilized as erosion and oxidation resistant coatings on turbine airfoils. Cruse *et al.* [14] described improvements of toughness in Cr₃Si alloyed with Mo, with possibilities of improved high temperature properties. Raj *et al.* [15] also reported improvements in creep properties of Cr₃Si when alloyed with Mo. Mo in all cases sits in the place of Cr. Gali *et al.* [12] showed that addition of very small levels of Re and Ce can slow down the coarsening rate at high temperatures. Both elements substitute Cr in the structure.

Looking at the improvements made by doping the material, a first-principles study on the mechanical properties of cubic Cr₃Si alloys can prove informative in future endeavors. This study aims to systematically investigate the effect of Ge, Ga, and Al doping on the mechanical properties of Cr₃Si using first-principles calculations. Ge was incorporated into the material in one previous study [9] and a theoretical look at the mechanical behavior of the alloy would provide better understanding. Al is chosen as it has shown to have significant effects on the decrease of electrical resistivity and increase of thermoelectric efficiency in high temperatures when alloyed in small concentrations with CrSi₂ binary silicide [16]. Given the promising results of Ge and Al doping in binary silicides, Ga could potentially portray similar properties. Al and Ge have shown preference to substitute on Si sites. All three elements are therefore substituted exclusively with

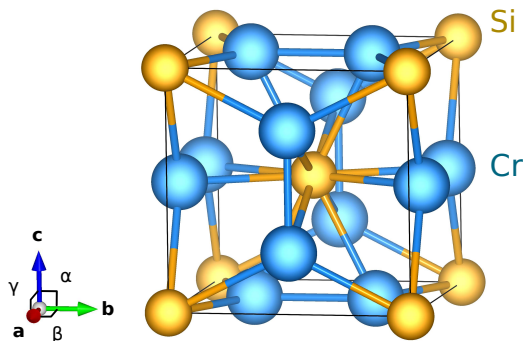


FIG. 1. The 8-atom conventional unitcell of Cr_3Si . Silicon atoms are shown in yellow, while chromium atoms are shown in blue, as indicated.

Si in our set of calculations. By analyzing changes in elastic moduli, wave velocities, Debye temperature, and anisotropy indices, we seek to provide a detailed understanding of the structural stability and mechanical behavior of these doped alloys. The insights gained from this research will guide the design of Cr_3Si -based materials with tailored properties for specific high-performance applications. This article is organized as follows. The details of the calculations are described in Sec. II, while the results and needed discussion is given in Sec. III. The article is then concluded in Sec. IV.

TABLE I. Calculated and experimental [18] lattice parameters for the 8-atom conventional cell of Cr_3Si .

	Calc. (GGA)	Calc. (HSE)	Exp.
a (Å)	4.50	4.43	4.57

II. COMPUTATIONAL METHODOLOGY

Density functional theory (DFT) [22, 23] calculations using the projector augmented wave (PAW) [24, 25] method is employed as implemented in the Vienna ab initio simulation package (VASP) [26]. The exchange correlation energy is described through the generalized gradient approximation (GGA) of Perdew-Burke-Ernzerhof (PBE) [27]. Hybrid functional of Heyd-Scuseria-Ernzerhof (HSE) [28] is also used for preliminary tests on the unitcell, with the standard mixing parameter of $\alpha = 0.25$. The plane wave basis is used with the 600 eV energy cut-off and the Hellmann-Feynman forces on each atom are converged to 0.001 eV/Å. The smearing method of Methfessel-Paxton is used in the calculations and smearing width of 0.2 eV is selected. Self-consistent calculations are considered to be converged when the energy convergence is less than 10^{-5} eV. Valence electrons of Cr $3s^23p^63d^54s^1$, Si $3s^23p^2$, Ge $3d^{10}4s^24p^2$, Ga $3d^{10}4s^24p^2$, and Al $3s^23p^1$ are adopted in PAW pseudopotentials. The first Brillouin zone is sampled by the

Γ -centered k-point mesh of $12 \times 12 \times 12$ in accordance with the Monkhorst-Pack scheme [29] for the conventional unitcell of Cr_3Si shown in Fig. 1. The atomic configurations for the study of the alloys at different compositions are generated using the Integrated Cluster Expansion Toolkit (ICET) [30]. To study the alloying effects at concentrations 12.5, 25, 37.5, and 50 at %, we used $\sqrt{2} \times \sqrt{2} \times \sqrt{3}$, $1 \times 1 \times 2$, $\sqrt{6} \times \sqrt{2} \times \sqrt{2}$, and $1 \times 1 \times 1$ supercells based on the conventional unitcell. Scaled down k-meshes are used for the corresponding supercells. The formulas used for calculating the mechanical properties are given in Appendix A.

III. RESULTS AND DISCUSSIONS

A. Electronic and mechanical properties of pristine Cr_3Si

Here, we discuss the electronic properties of pure Cr_3Si . We start from the experimental CIF [18] file and optimize the ionic positions as well as lattice vectors through DFT calculations. To this end, we consider the conventional unitcell which includes 8 ions as illustrated in Figure 1. Table I summarizes the experimental and DFT lattice parameters of pristine Cr_3Si . The obtained results show that system preserves its cubic symmetry after geometric optimization. In DFT, the accurate description of electron-electron correlation is contingent upon the choice of exchange-correlation functional [27, 31]. To determine the most suitable functional for further calculations, it is essential to compare the DFT results with corresponding experimental values. According to Table I, based on the comparison between the obtained lattice constants and experimental values, GGA calculations provide more accurate results than the HSE approach. Therefore, we proceed with deriving the material properties using GGA functional.

The calculated band structure of Cr_3Si along the X-R-M- Γ -R high-symmetry path is shown in Fig. 2. The energy bands are plotted relative to the Fermi level (E_F), set to 0 eV. The distinct band features observed indicate the metallic nature of Cr_3Si , with the Fermi level crossing several bands. This suggests that there are available electronic states at the Fermi level, contributing to the electrical conductivity of the material. The DOS plot provides a detailed view of the contributions from different atomic orbitals. The total DOS is shown alongside the partial DOS for Cr and Si atoms. The overall DOS shows significant contributions near the Fermi level, reinforcing the metallic nature of Cr_3Si . The partial DOS for Cr atoms indicates dominant d -orbital contributions near the Fermi level. This is expected as Cr d -electrons play a crucial role in the bonding and electronic properties of the material. The partial DOS for Si atoms shows contributions primarily from p -orbitals, with some hybridization with Cr d -orbitals. This hybridization is indicative of the strong covalent interactions between Cr and Si

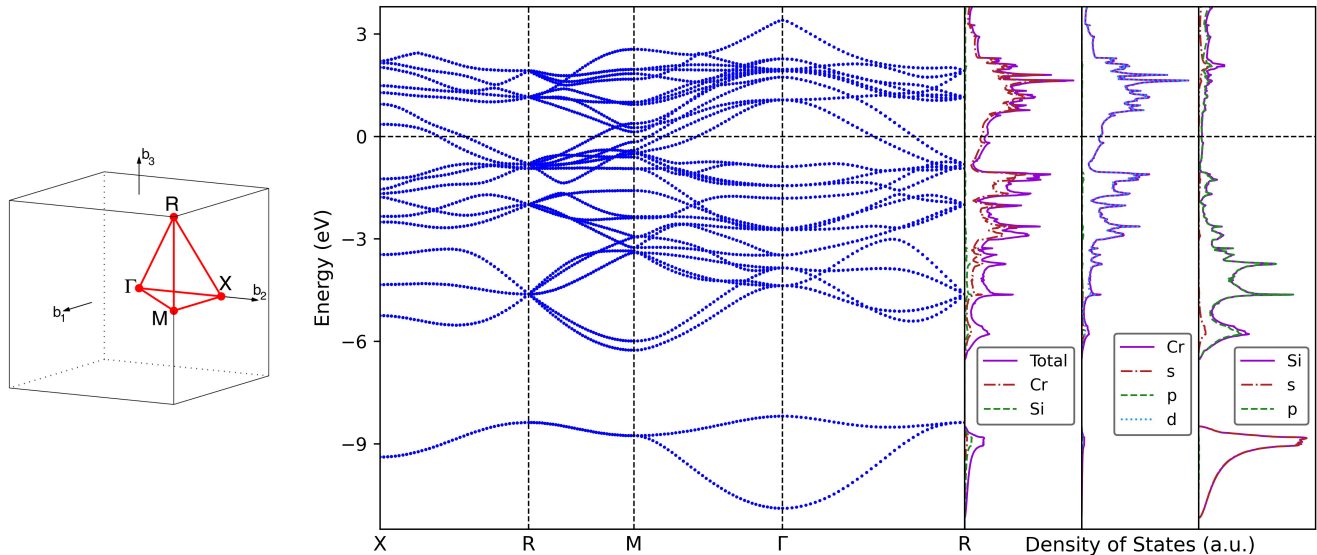


FIG. 2. Band structure of Cr_3Si alongside densities of state. The specific atomic orbitals contributing to the orbital-projected densities of states are indicated. The path of high-symmetry points considered in the first Brillouin zone is taken from Ref. [17]

TABLE II. Elastic constants of Cr_3Si shown alongside prior calculated and experimental values.

Method	Ref.	C_{11} (GPa)	C_{12} (GPa)	C_{44} (GPa)
VASP-PBE	This work	507.6	138.1	150.7
CASTEP-PBE	[19]	480.8	136.1	149.4
CASTEP-PBE	[20]	490.2	127.9	145.6
Exp.	[21]	416.0	98.7	129.0

atoms in the Cr_3Si structure. The calculated bands and DOS are in good agreement with previous calculations [19, 20, 32].

The mechanical properties of a material are fundamentally characterized by its elastic constants, including C_{11} (longitudinal stiffness), C_{12} (lateral stiffness), and C_{44} (twisting modulus). The elastic constant C_{11} quantifies the material's resistance to uniaxial stress applied along the principal crystallographic axes. In contrast, C_{12} describes the material's response to stress in one direction that induces strain in a perpendicular direction. The elastic constant C_{44} is crucial for understanding the material's resistance to shear deformation, thereby providing insights into its rigidity and ductility. Calculated elastic constants of Cr_3Si are presented in Table II along with elastic constants from previous calculations and experiment. The mechanical stability criteria for a cubic structure are $C_{11} > 0$, $C_{44} > 0$, and $C_{11} - C_{12} > 0$. These criteria are all satisfied for pristine Cr_3Si . The discrepancies between theoretical and experimental values are typical and can be attributed to various factors. In experimental samples, imperfections such as vacancies, dislocations, and grain boundaries are present, which are not accounted for in idealized theoretical models. Additionally, the presence of thermal vibrations at the experimental measurement temperature can

lead to reduced elastic constants compared to 0 K calculations. The higher elastic constants in Cr_3Si also suggest that it could be more suitable for high-stress applications compared to other Cr-Si compounds, which may have lower stiffness and potentially higher ductility. Among the $X_3\text{Si}$ ($X = \text{V}, \text{Nb}, \text{Cr}, \text{Mo}$ and W) compounds analyzed [33], Cr_3Si demonstrates the highest shear modulus (158.9 GPa) and bulk modulus (248.7 GPa), outperforming V_3Si , Nb_3Si , and Mo_3Si , which exhibit lower values across these parameters [33]. Notably, while Mo_3Si shows a comparable bulk modulus (249.2 GPa), it presents a reduced shear modulus (134.6 GPa), suggesting that Cr_3Si offers superior stiffness and enhanced resistance to shear deformation. These mechanical properties render Cr_3Si the hardest compound in the series, with a hardness of 10.96 GPa. Consequently, Cr_3Si emerges as one of the most mechanically robust $X_3\text{Si}$ compounds, making it particularly suitable for high-stress applications. In contrast, Nb_3Si , with a lower bulk modulus (175.0 GPa) and hardness (5.72 GPa), may be more ductile but lacks the stiffness required for such demanding environments.

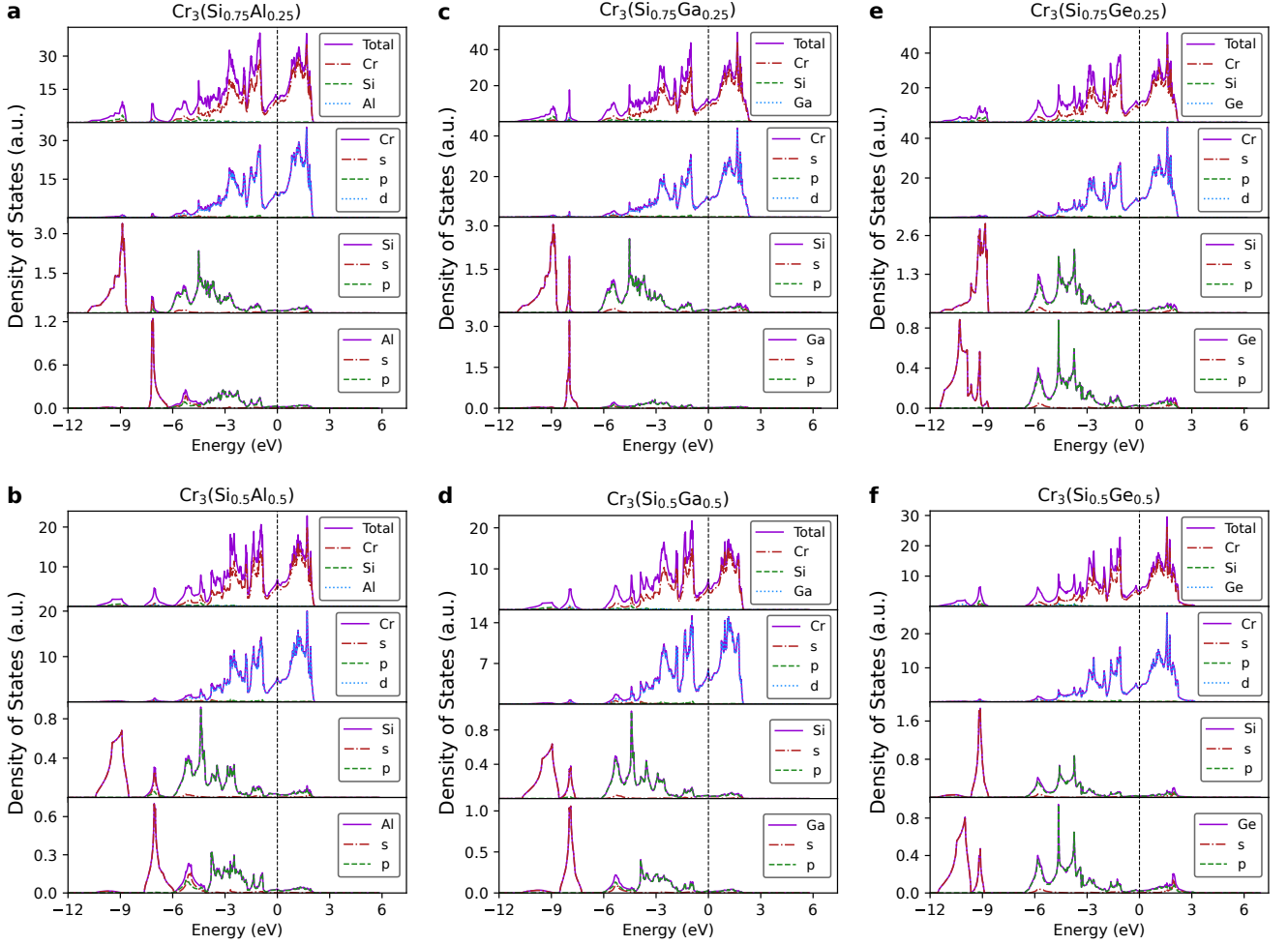


FIG. 3. The DOS of doped Cr_3Si at alloy concentrations of 25% and 50%. The DOS plots reveal the contributions of dopants (Ge, Ga, and Al) to the electronic structure.

B. Electronic properties of doped- Cr_3Si

Following the examination of the mechanical properties of pristine Cr_3Si , we explore potential enhancements through doping with Al, Ga, and Ge. This section focuses on the DOS of the doped systems, with particular attention to the modifications in electronic properties, especially in the vicinity of the Fermi level. Fig. 3 shows DOS of Doped Cr_3Si in two different alloy concentrations of 25 and 50 at %. For both 25 and 50 Al doping concentrations, the DOS maintains a metallic character with significant states at the Fermi level. The Cr d -orbitals continue to dominate near the Fermi level, similar to pristine Cr_3Si . This indicates that the primary electronic structure is retained even with Al doping. The Al s and p orbitals contribute to the DOS but do not significantly alter the overall distribution near the Fermi level, suggesting that Al's influence on the electronic structure is additive rather than transformative. We see similar behavior for both Ga and Ge, where the metallic character

of the structure is maintained in the alloys, with small contributions from the dopants' orbitals

Retention of metallic character indicates that doping with these elements does not disrupt the fundamental electronic structure responsible for metallic conductivity. The dominance of Cr d -orbital contributions near the Fermi level remains consistent from the pristine state (Fig. 2) through the various doped states. This suggests that the core electronic properties of the Cr_3Si matrix are preserved despite the incorporation of dopants. The similarities between the DOS of doped and pristine Cr_3Si in primary peaks and hybridization patterns indicate that these dopants integrate into the lattice without drastically altering the electronic interactions that define Cr_3Si 's properties.

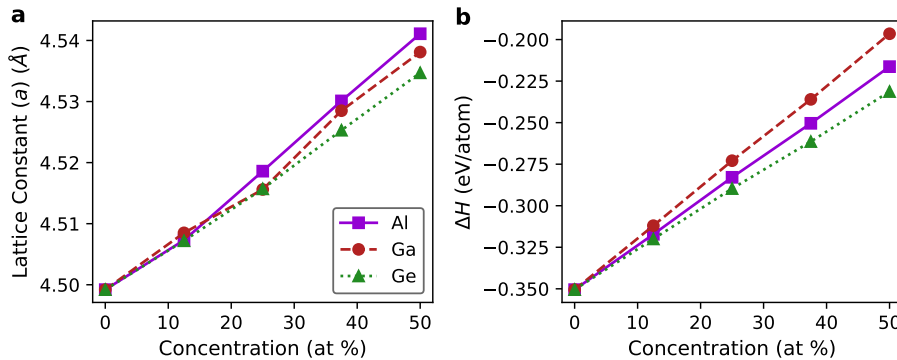


FIG. 4. (a) Lattice constants and (b) formation enthalpies of doped Cr_3Si as a function of alloy concentration.

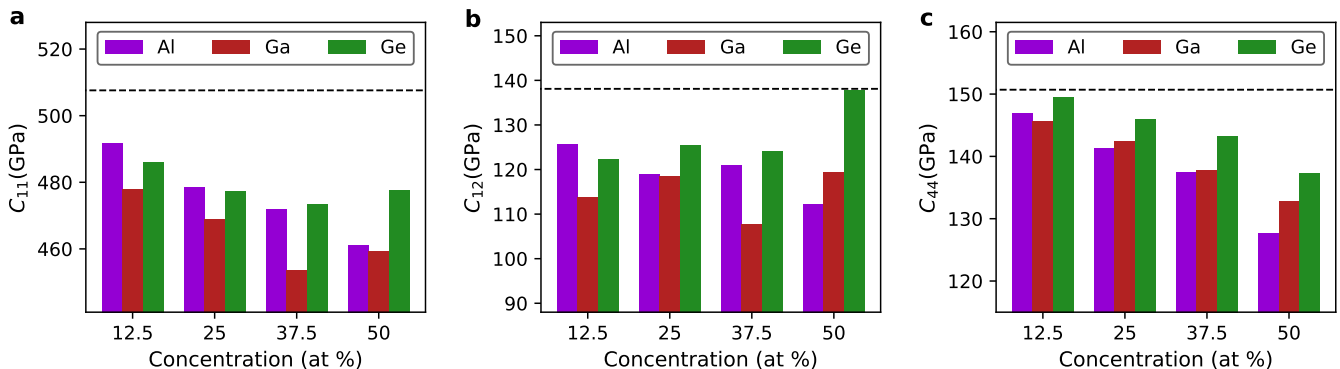


FIG. 5. Elastic constants of Cr_3Si doped with Ge, Ga, and Al as a function of alloy concentration. The dotted line shows the calculated elastic constant for the pristine structure.

C. Mechanical properties of doped- Cr_3Si

To manipulate the mechanical properties of pristine Cr_3Si , one effective approach is to introduce relevant dopants such as Al, Ge, and Ga into the system. In this section, we explore how these dopants influence the mechanical properties of Cr_3Si and discuss the resulting changes in material behavior. In this regard, the first step is to check how the system expands or reduces the lattice constants with doping. Fig. 4 (a) illustrates the variation in lattice constants of Cr_3Si as a function of alloy concentration for different dopants (Al, Ga, Ge). The lattice constants are shown to increase uniformly with the addition of each dopant. The observed increase in lattice constants with dopant concentration reflects the accommodation of larger dopant atoms within the Cr_3Si structure, leading to lattice expansion. This structural change can impact the mechanical properties of the material, such as its ductility and hardness.

It is crucial to investigate whether the system is stable after doping or not. Fig. 4 (b) presents the formation enthalpies of Cr_3Si alloys as a function of dopant concentration. Formation enthalpy is a critical measure of the thermodynamic stability of the alloys. Formation enthalpy of undoped Cr_3Si is -0.35 eV/atom, in agree-

ment with the experimental value of -0.36 eV/atom [18]. The consistent negative formation enthalpies across all doped configurations suggest that these alloys are stable, although the degree of stability decreases with higher dopant concentrations. This information is crucial for understanding the trade-offs between structural stability and the desired modifications in material properties through doping.

We now discuss how doping can tune the mechanical properties of cubic Cr_3Si . A comparison of the elastic constants of doped Cr_3Si is given in Fig. 5. The graphs show the impact of doping on the stiffness and shear resistance of Cr_3Si , with the trends indicating how the introduction of these elements alters the material's mechanical properties. The consistent decrease in C_{11} (longitudinal stiffness), C_{12} (lateral stiffness) and C_{44} (twisting modulus) across all doped configurations suggests that doping generally reduces the mechanical stiffness and shear resistance of Cr_3Si . This trend can be attributed to the larger atomic radii of the dopants (Ge, Ga, and Al) compared to Si, leading to lattice expansion and a subsequent weakening of the material's bonding interactions. The most significant reductions are observed with Ga doping, making it the most effective at increasing ductility but also the most detrimental to the material's stiffness and

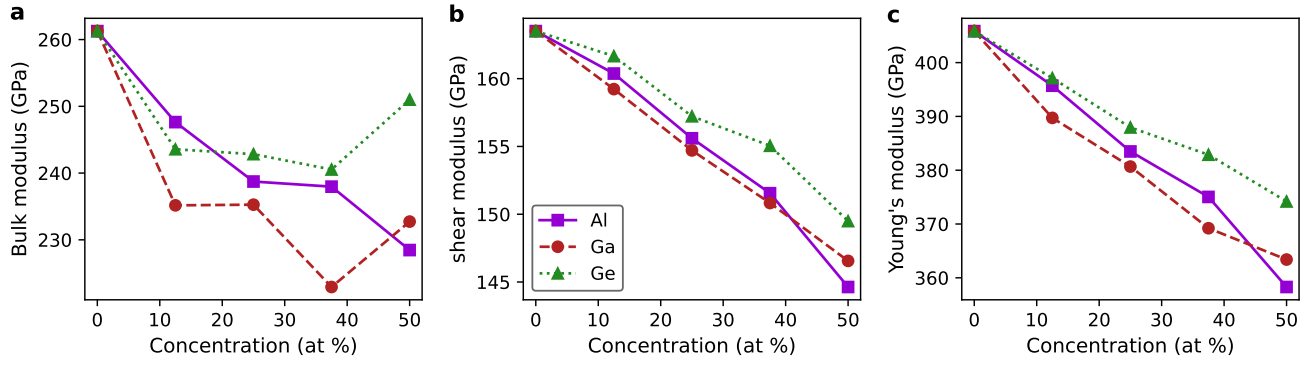


FIG. 6. Elastic moduli of doped Cr_3Si as a function of alloy concentration: (a) bulk modulus, (b) shear modulus, and (c) Young's modulus.

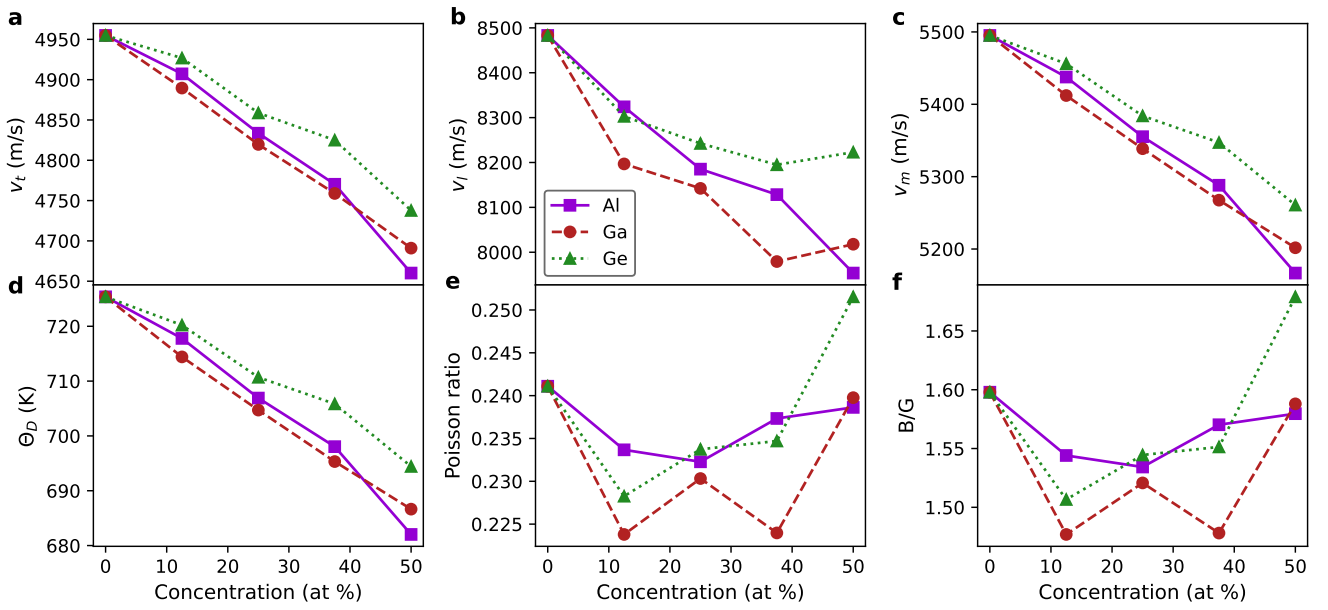


FIG. 7. (a) Transverse wave velocity, (b) longitudinal wave velocity, (c) average wave velocity, (d) Debye temperature, (e) Poisson ratio, and (f) B/G ratio of doped Cr_3Si as a function of alloy concentration.

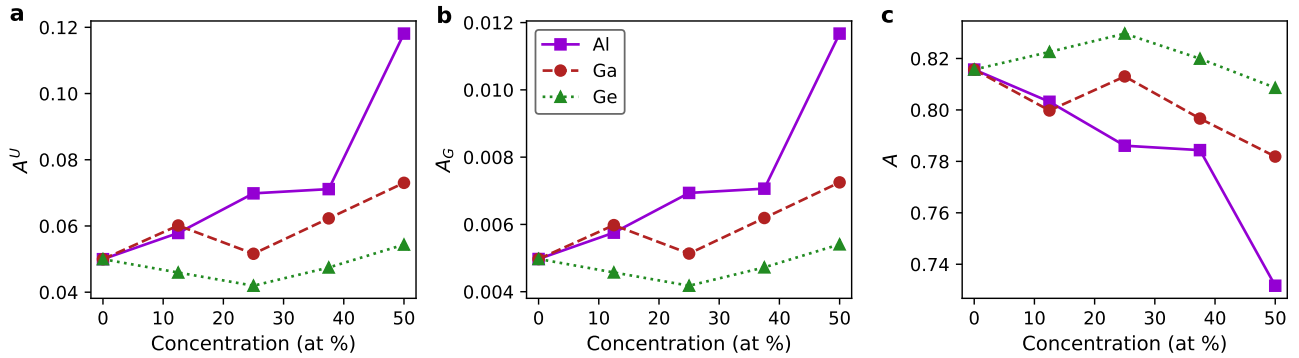


FIG. 8. Mechanical anisotropic indices of doped Cr_3Si : (a) universal anisotropic index, (b) percent anisotropy of shear modulus, and (c) shear anisotropic factor.

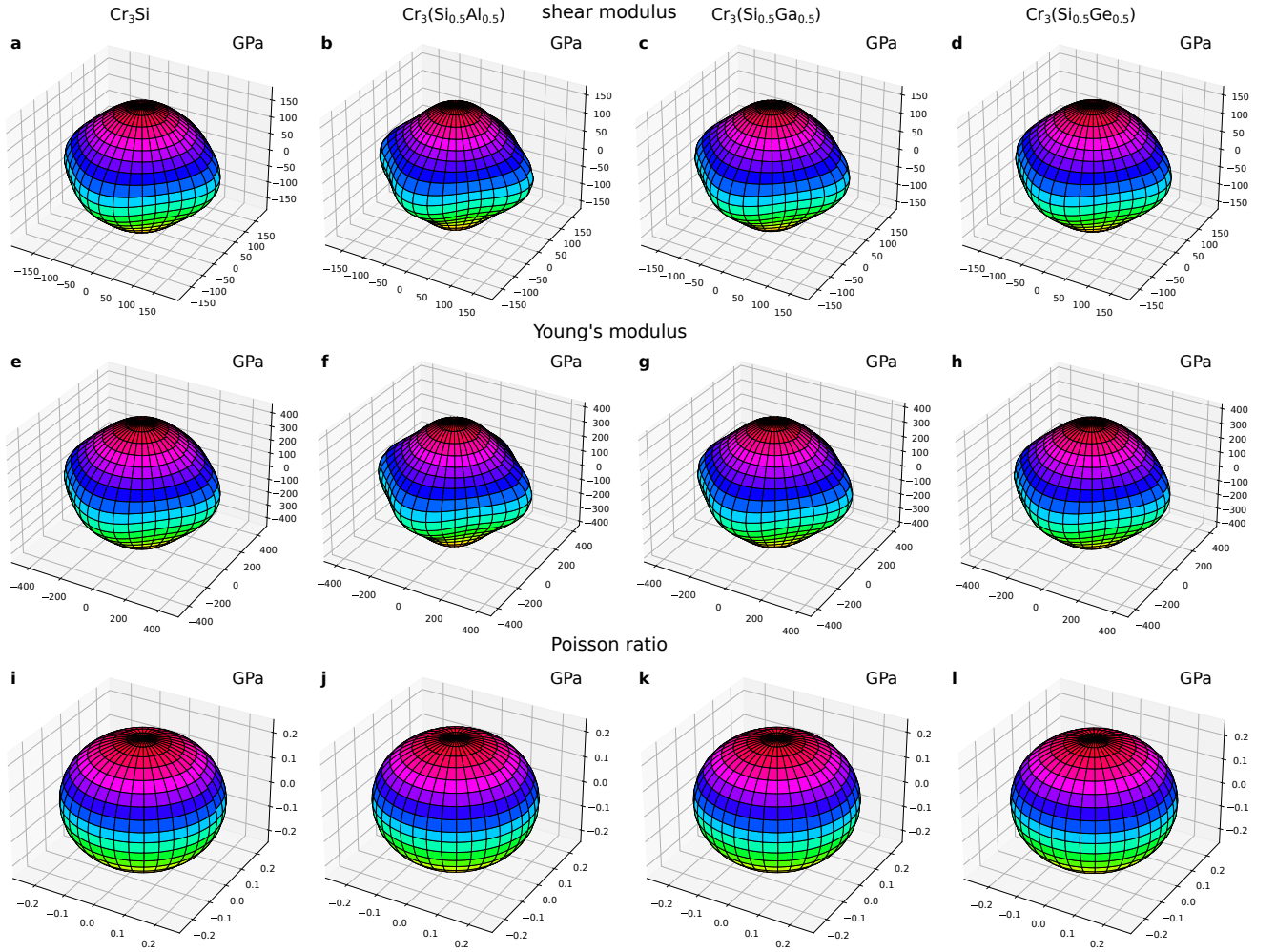


FIG. 9. Three dimensional contours of (a)-(d) the shear modulus, (e)-(h) Young's modulus, and (i)-(l) Poisson ratio of doped Cr_3Si . The distance between zero and any point on the surfaces is equal to the elastic modulus or Poisson ratio in that direction.

shear resistance. Through these elastic constants, we can find the elastic moduli and subsequently the wave velocities, Debye temperature, and anisotropic indices. This incorporation is explicitly formulated in Appendix A.

The deformation of the material under force can be further examined by looking at the elastic moduli. Fig. 6 presents the elastic moduli (bulk modulus B , shear modulus G , and Young's modulus E) of Cr_3Si doped with Al, Ga, and Ge at various concentrations. These moduli provide insights into the mechanical properties and the stiffness of the material. Bulk modulus decreases almost linearly with increasing the Al concentration, indicating a reduction in the material's resistance to uniform compression. This suggests that Cr_3Si becomes more compressible and less stiff as more Al is incorporated. Ga shows a similar downward trend, though with more pronounced fluctuations, especially at higher concentrations. This variability may be due to the specific interaction of Ga atoms within the Cr_3Si matrix. The bulk modulus of Ge-doped Cr_3Si also decreases, but the trend is

less steep compared to Al and Ga. This implies that Ge doping results in a slightly more stable structure in terms of compressibility compared to Al and Ga. For all three dopants, the shear modulus decreases with increasing concentration. Shear modulus is crucial for understanding the material's response to shear stress. Both Al and Ga show significant decrease in shear modulus, indicating that doping with these elements reduces the material's rigidity and makes it more susceptible to shear deformation. Ge also reduces shear modulus, but the reduction is less pronounced compared to Al and Ga. This suggests that Ge-doped Cr_3Si retains more of its original rigidity. The Young's modulus, which measures the stiffness of a material under uniaxial stress, decreases steadily with increasing Al concentration. This reduction reflects a decrease in the material's overall stiffness. Similar to shear modulus, Ga-doped Cr_3Si exhibits a decline in the Young's modulus with increasing concentration, highlighting the reduced stiffness. The decrease in the Young's modulus for Ge-doped Cr_3Si is more gradual,

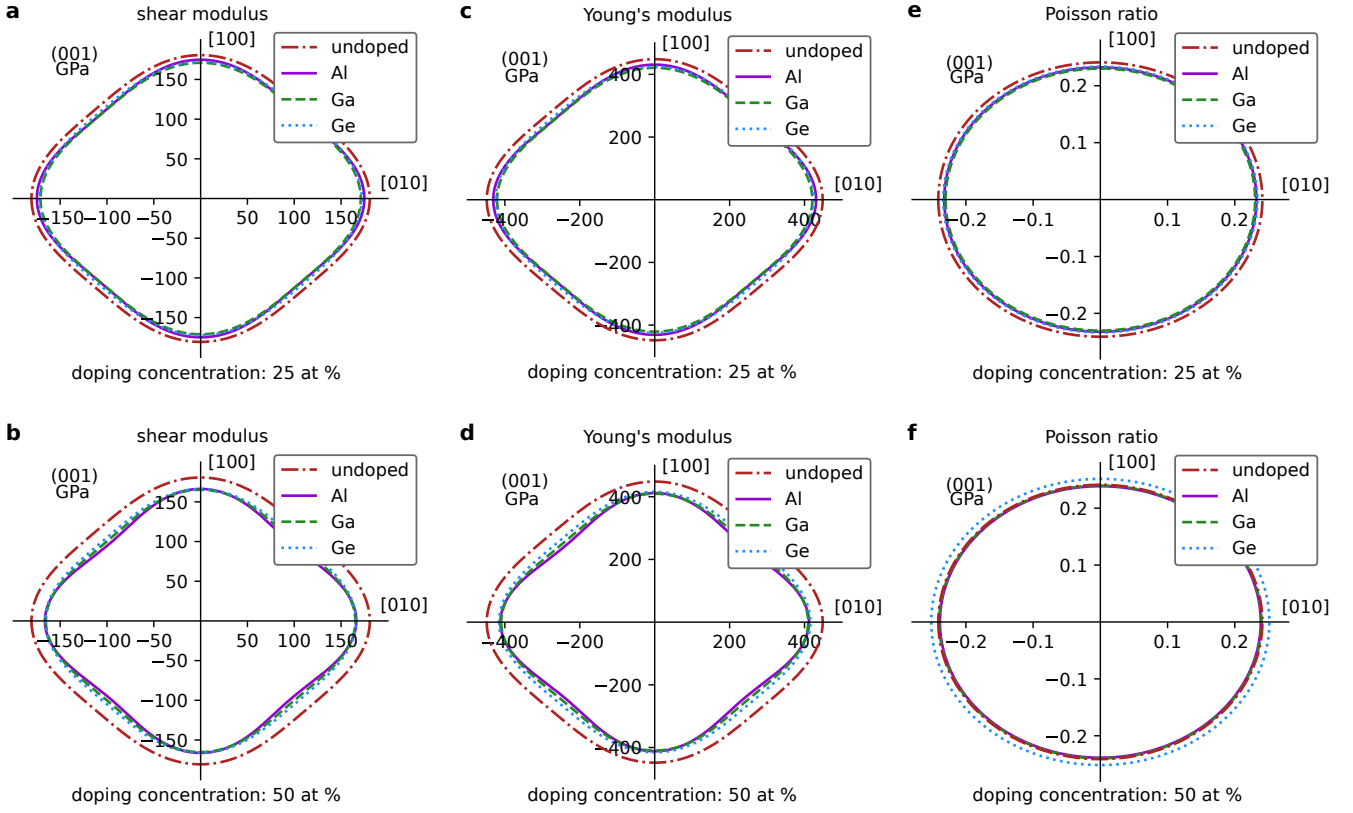


FIG. 10. Two dimensional projections of (a),(b) the shear modulus, (c),(d) Young's modulus, and (e),(f) Poisson ratio of doped Cr_3Si .

indicating that the material retains a higher degree of stiffness compared to Al and Ga doping.

The consistent decrease in all three elastic moduli with increasing dopant concentration across Al, Ga, and Ge indicates that doping generally reduces the mechanical stiffness and rigidity of Cr_3Si . This trend can be attributed to the larger atomic radii of the dopants, which cause lattice expansion and disrupt the original bonding interactions within the Cr_3Si matrix. The reduction in mechanical strength suggests that heavily doped Cr_3Si may be less suitable for applications requiring high stiffness, and resistance to deformation. However, these materials might still be valuable in applications where reduced stiffness is advantageous or where other properties (such as thermal stability or electrical conductivity) are more critical. By carefully controlling the type and concentration of dopants, it may be possible to tailor the mechanical properties of Cr_3Si for specific applications. For instance, moderate doping levels could achieve a balance between maintaining sufficient mechanical strength while enhancing other desirable properties.

Fig. 7 shows the transverse wave velocity (v_t), longitudinal wave velocity (v_l), average wave velocity (v_m), and Debye temperature for Cr_3Si doped with Al, Ga, and Ge at various concentrations. These properties provide insights into the mechanical and thermal behavior of the

doped materials. The transverse wave velocity, which relates to shear deformation, consistently decreases with increasing dopant concentration for all three dopants. The longitudinal wave velocity, associated with compressional waves, shows a decrease with increased dopant concentration for all dopants, but the trend is less uniform compared to v_t . The average wave velocity, a composite measure of v_t and v_l , also decreases with higher dopant concentrations for all dopants. The Debye temperature, which correlates with the material's stiffness and thermal properties, follows the same downward trend with increasing dopant concentration. The consistent reduction in wave velocities and Debye temperature with higher dopant concentrations indicates that doping generally softens the Cr_3Si , making it less rigid and more prone to deformation. This is aligned with the trends observed in the elastic moduli (Fig. 6), further reinforcing the impact of doping on mechanical strength. The decrease in Debye temperature suggests that the thermal conductivity of doped Cr_3Si alloys is reduced. This can be attributed to the larger atomic sizes of the dopants, which disrupt the phonon propagation and reduce thermal conductivity. While the reduced stiffness might limit structural applications, the altered thermal properties could make doped Cr_3Si suitable for thermal barrier coatings or other high-temperature applications.

Brittleness or ductility of an alloy can be determined using B/G and Poisson (ν) ratios [34]. If B/G is higher than 1.75 and ν is higher than 0.26, the material under investigation is ductile and has strong metallic character, while lower values than the reference points mentioned suggest brittleness. Fig. 7 (e) and (f) show ν and B/G as a function of alloy concentration. The trends for both parameters are quite similar, with the numbers suggesting brittleness of doped Cr_3Si all throughout different percentages. Higher doping concentrations of Ge make the alloy more ductile, while Al-doped Cr_3Si is less prone to change in the studied range.

Mechanical anisotropic indices provide insight into elastic anisotropy, which is key for understanding the material's behavior under different directional stresses. Fig. 8 visualizes these indices for Cr_3Si doped with Al, Ga, and Ge at various concentrations. The universal anisotropic index (A^U) quantifies the overall elastic anisotropy of the material, while the percent anisotropy of the shear modulus (A_G) measures the directional dependence of shear stiffness. Higher values of A^U and A_G indicate greater anisotropy of the structure. The shear anisotropic factor (A) provides a measure of how the shear modulus varies with crystallographic direction. A value of $A = 1$ indicates isotropy, while values deviating from 1 signify anisotropy. The increase in anisotropic indices (A^U , A_G , and A) with higher concentrations of Al and Ga suggests that these dopants introduce significant directional dependence in the mechanical properties of Cr_3Si . This anisotropy can influence the material's response to mechanical stresses, potentially leading to uneven deformation or failure along specific crystallographic directions. Materials with high anisotropy might be less suitable for structural applications where isotropic properties are critical for uniform load distribution. Applications that can benefit from directional mechanical properties might leverage higher anisotropy, while those requiring uniform strength might limit doping concentrations. Fig. 9 shows the three dimensional surfaces of G , E , and ν for pristine and doped Cr_3Si . Dopants Ge and Ga generate slight changes in the crystal's anisotropy, as we predicted from the anisotropic indices of the alloys. Al creates the most significant changes in the material's anisotropy among the three studied elements when going to higher percentages of doping. This is sufficiently visible when looking at the three dimensional contours of the elastic moduli. To see these changes more clearly, the two dimensional projections of G , E , and ν are given in Fig. 10 on the (001) plane at 25 % and 50 % alloy concentrations. Besides the alterations in anisotropy by Al, we can also see distinctly that Ge raises ν at high doping percentages.

IV. CONCLUSION

This study comprehensively investigated the effects of Ge, Ga, and Al doping on the mechanical properties and

anisotropy of cubic Cr_3Si using first-principles calculations. Our findings reveal that doping with these elements leads to an increase in lattice constants, indicative of lattice expansion due to the larger atomic radii of the dopants. Despite the negative formation enthalpies observed across all doped configurations, indicating overall thermodynamic stability, the mechanical stiffness and rigidity of Cr_3Si decrease with increasing dopant concentration. This is evidenced by the reduction in bulk modulus, shear modulus, and Young's modulus across the doped samples, suggesting that the material becomes softer and less resistant to deformation as doping concentration increases. This study further highlights the impact of doping on the mechanical anisotropy of Cr_3Si . Al and Ga doping significantly increase the anisotropy indices, suggesting that these dopants introduce considerable directional dependence in the mechanical properties. This enhanced anisotropy could lead to uneven deformation under stress, particularly in applications requiring uniform mechanical strength. In contrast, Ge doping maintains a relatively isotropic behavior, making it a more favorable candidate for applications that demand balanced mechanical and thermal properties. The wave velocities and Debye temperature analyses further support the conclusion that doping generally softens the Cr_3Si structure, with potential implications for its thermal conductivity. The consistent retention of metallic character across all doped configurations, as indicated by the DOS analyses, suggests that the core electronic properties of Cr_3Si are preserved despite the introduction of dopants. This retention is crucial for applications where electrical conductivity is essential.

In summary, while Ge, Ga, and Al doping can be employed to tailor specific properties of Cr_3Si , such as thermal stability and oxidation resistance, these modifications generally come at the cost of reduced mechanical strength and increased anisotropy. Ge emerges as the most balanced dopant, offering a trade-off between maintaining structural integrity and enhancing other functional properties. These insights provide a valuable foundation for the future design and optimization of Cr_3Si -based materials, particularly for high-performance applications where directional mechanical properties and thermal stability are of paramount importance.

V. ACKNOWLEDGMENTS

We gratefully acknowledge fruitful discussions with S. Mu. Use was made of computational facilities purchased with funds from the National Science Foundation (CNS-1725797) and administered by the Center for Scientific Computing (CSC). The CSC is supported by the California NanoSystems Institute and the Materials Research Science and Engineering Center (MRSEC; NSF DMR 2308708) at UC Santa Barbara.

VI. CONFLICT OF INTEREST

The authors declare no conflict of interest.

VII. DATA AVAILABILITY STATEMENT

The data that support the findings of this study are available from the corresponding author upon reasonable request.

Appendix A: Calculation of mechanical properties

The structural stability of a doped system can be determined through formation enthalpy calculation using the following formula [35]:

$$\Delta H_{\text{Cr}_i\text{Si}_j\text{X}_k} = \frac{1}{i+j+k} (E_{\text{Cr}_i\text{Si}_j\text{X}_k} - i \times E_{\text{Cr}} - j \times E_{\text{Si}} - r \times E_{\text{X}}), \quad (\text{A1})$$

where i, j, k are the molar fractions of Cr, Si, and the alloying elements X in the alloy, $E_{\text{Cr}}, E_{\text{Si}}, E_{\text{X}}$ are the energies of pure elements, and $E_{\text{Cr}_i\text{Si}_j\text{X}_k}$ is the energy of the corresponding alloy.

The bulk and shear moduli of a cubic structure can be evaluated using the Voigt-Reuss-Hill (VRH) approximation. The VRH approximation is the average of the lower bound of Voigt and upper bound of Reuss, providing the methodology to connect elastic constants to mechanical properties of crystalline materials. These moduli are obtained as follows [36]:

$$B = B_V = B_R = \frac{C_{11} + 2C_{12}}{3}, \quad (\text{A2})$$

$$G_V = \frac{C_{11} - C_{12} + 3C_{44}}{5}, \quad (\text{A3})$$

$$G_R = \frac{5(C_{11} - C_{12})C_{44}}{3(C_{11} - C_{12}) + 4C_{44}}, \quad (\text{A4})$$

$$G = \frac{G_V + G_R}{2}. \quad (\text{A5})$$

C_{ij} in the above formulas are the calculated elastic constants of the alloys. $B_V, B_R,$ and B are the bulk moduli calculated by Voigt, Reuss, and Voigt-Reuss-Hill approximation, respectively. $G_V, G_R,$ and G are the shear moduli calculated by Voigt, Reuss, and Voigt-Reuss-Hill approximation, respectively. The isotropic Young's modulus E can then be calculated as:

$$E = \frac{9BG}{3B + G}. \quad (\text{A6})$$

The isotropic Poisson ratio ν is evaluated through:

$$\nu = \frac{3B - 2G}{2(3B + G)}. \quad (\text{A7})$$

The wave velocities and the Debye temperature Θ_D can be determined using the mechanical properties [37]:

$$v_t = \left(\frac{G}{\rho}\right)^{\frac{1}{2}}, \quad (\text{A8})$$

$$v_l = \left(\frac{B + \frac{4}{3}G}{\rho}\right)^{\frac{1}{2}}, \quad (\text{A9})$$

$$v_m = \left[\frac{1}{3}\left(\frac{1}{v_l^3} + \frac{2}{v_t^3}\right)\right]^{-\frac{1}{3}}, \quad (\text{A10})$$

$$\Theta_D = \frac{h}{k_B} \left[\frac{3n}{4\pi} \left(\frac{N_A \rho}{M}\right)\right]^{\frac{1}{3}} v_m, \quad (\text{A11})$$

where $v_t, v_l,$ and v_m are transverse, longitudinal, and average wave velocities; n is the number of atoms per formula, M is the molecular weight, ρ is the density and $h, k_B,$ and N_A are the Avagadro's, Planck's, and Boltzmann constants, respectively.

Elastic anisotropy of a material can be characterized through several anisotropic indices [38–40]:

$$A^U = \frac{5G_V}{G_R} + \frac{B_V}{B_R} - 6, \quad (\text{A12})$$

$$A_B = \frac{B_V - B_R}{B_V + B_R}, \quad (\text{A13})$$

$$A_G = \frac{G_V - G_R}{G_V + G_R}, \quad (\text{A14})$$

$$A = \frac{2C_{44}}{C_{11} - C_{12}}. \quad (\text{A15})$$

Here A^U is the universal anisotropic index, A_B and A_G are the percent anisotropy of the bulk and shear modulus, and A is the shear anisotropic factor. Elastic anisotropy can provide needed insight for the applications of doped Cr_3Si as it connects directly to the production of micro cracks inside the material. The formation and propagation of these cracks influence the usage of the doped compounds as structural materials at elevated temperatures.

Elastic anisotropy can be further investigated as a function of crystallographic orientation using the three dimensional surface of an elastic modulus. E of a crystal

with cubic structure is formulated as [41]:

$$\frac{1}{E} = S_{11} - 2(S_{11} - S_{12} - \frac{1}{2}S_{44})(l_1^2l_2^2 + l_1^2l_3^2 + l_2^2l_3^2), \quad (\text{A16})$$

where S_{ij} are the elastic compliance constants; and l_1 , l_2 , and l_3 are the direction cosines. We can also calculate ν and G in different directions using spherical coordinates. This can be done by combining this equation and Eqs. A6 and A7.

-
- [1] X. Chen and C. Liang, *Catal. Sci. Technol.* **9**, 4785 (2019).
- [2] J. Dshemuchadse and W. Steurer, *Inorg. Chem.* **54**, 1120 (2015).
- [3] K. Ioroi, I. Ohnuma, X. Xu, R. Kainuma, and T. Omori, *Calphad* **85**, 102690 (2024).
- [4] H. P. J. Wijn, in *Magnetic Properties of Metals*, Data in Science and Technology (Springer-Verlag, Berlin, 1991).
- [5] J. E. Jørgensen, J. D. Axe, L. M. Corliss, and J. M. Hastings, *Phys. Rev. B* **25**, 5856 (1982).
- [6] I. G. Mihailov, W. M. Pan, A. D. Shevtshenko, and G. Ber, *Solid State Phys.* **21**, 2797 (1979).
- [7] D. L. Anton and D. M. Shah, *MRS Online Proceedings Library* **213**, 733 (1990).
- [8] S. Raj, *Mater. Sci. Eng.: A* **192-193**, 583 (1995).
- [9] A. Soleimani-Dorcheh and M. C. Galetz, *Oxid. Met.* **84**, 73 (2015).
- [10] A. Soleimani-Dorcheh, W. Donner, and M. C. Galetz, *Mater. Corros.* **65**, 1143 (2014).
- [11] D. Shah and D. Anton, *Mater. Sci. Eng.: A* **153**, 402 (1992).
- [12] A. Gali, H. Bei, and E. George, *Acta Mater.* **57**, 3823 (2009).
- [13] S. Raj, *Mater. Sci. Eng.: A* **201**, 229 (1995).
- [14] T. Cruse and J. Newkirk, *Mater. Sci. Eng.: A* **239-240**, 410 (1997), 4th Conference on High-Temperature Intermetallics.
- [15] S. Raj, J. Daniel Whittenberger, B. Zeumer, and G. Sauthoff, *Intermetallics* **7**, 743 (1999).
- [16] Z. Pan, L. Zhang, and J. Wu, *Scr. Mater.* **56**, 245 (2007).
- [17] W. Setyawan and S. Curtarolo, *Comp. Mater. Sci.* **49**, 299 (2010).
- [18] S. Cui and I.-H. Jung, *J. Alloys Compd.* **708**, 887 (2017).
- [19] B. Ren, D.-H. Lu, R. Zhou, D.-P. Ji, M.-Y. Hu, and J. Feng, *Chin. Phys. B* **27**, 107102 (2018).
- [20] H. Wei, Y. L. Chen, and L. Su, in *Functional and Functionally Structured Materials II*, Materials Science Forum, Vol. 913 (Trans Tech Publications Ltd, 2018) pp. 596–606.
- [21] H. Bei, E. George, and G. Pharr, *Scr. Mater.* **51**, 875 (2004).
- [22] W. Kohn and L. J. Sham, *Phys. Rev.* **140**, A1133 (1965).
- [23] P. Hohenberg and W. Kohn, *Phys. Rev.* **136**, B864 (1964).
- [24] P. E. Blöchl, *Phys. Rev. B* **50**, 17953 (1994).
- [25] G. Kresse and D. Joubert, *Phys. Rev. B* **59**, 1758 (1999).
- [26] G. Kresse and J. Furthmüller, *Comp. Mater. Sci.* **6**, 15 (1996).
- [27] J. P. Perdew, K. Burke, and M. Ernzerhof, *Phys. Rev. Lett.* **77**, 3865 (1996).
- [28] J. Heyd, G. E. Scuseria, and M. Ernzerhof, *J. Chem. Phys.* **118**, 8207 (2003).
- [29] H. J. Monkhorst and J. D. Pack, *Phys. Rev. B* **13**, 5188 (1976).
- [30] M. Ångqvist, W. A. Muñoz, J. M. Rahm, E. Fransson, C. Durniak, P. Rozyczko, T. H. Rod, and P. Erhart, *Adv. Theory Simul.* **2**, 1900015 (2019).
- [31] A. J. Cohen, P. Mori-Sánchez, and W. Yang, *Science* **321**, 792 (2008).
- [32] Y. Pan, D. Pu, and E. Yu, *Vacuum* **185**, 110024 (2021).
- [33] H. Wei, Y. L. Chen, and L. Su, in *Materials Science Forum*, Vol. 913 (Trans Tech Publ, 2018) pp. 596–606.
- [34] S. Pugh, *Lond. Edinb. Dubl. Phil. Mag.* **45**, 823 (1954).
- [35] A. Zoroddu, F. Bernardini, P. Ruggerone, and V. Fiorentini, *Phys. Rev. B* **64**, 045208 (2001).
- [36] P. Söderlind, O. Eriksson, J. M. Wills, and A. M. Boring, *Phys. Rev. B* **48**, 5844 (1993).
- [37] O. L. Anderson, *J. Phys. Chem. Solids* **24**, 909 (1963).
- [38] C. Zener, in *Elasticity and anelasticity of metals* (University of Chicago Press, 1991).
- [39] F. W. Vahldiek and S. A. Mersol, in *Anisotropy in Single-Crystal Refractory Compounds*, Metallic Materials (Springer New York, NY, 1968).
- [40] S. I. Ranganathan and M. Ostojia-Starzewski, *Phys. Rev. Lett.* **101**, 055504 (2008).
- [41] J. F. Nye, in *Physical Properties of Crystals* (Oxford University Press, Oxford, 1985).